Viser Technology Pte. Ltd.
Research and Application of Materials Science
doi: 10.33142/rams.v2i2.3170

Research Article Open Access

Effect of Carbides and γ/γ' Eutectic on Crack Initiation and Propagation in Ni-based Superalloy

Junwei QIN[1], Xiaohua CHEN[2*], Kaixuan CHEN[1], Xinghai YANG[1], Weiyang XIE[2], Yanlin WANG[1], Zidong WANG[1*]

1 School of Science and Engineering, University of Science and Technology Beijing, Beijing, China
2 State Key Laboratory for Advanced Metals and Materials, University of Science and Technology Beijing, Beijing, China

***Corresponding Author:** Xiaohua CHEN, E-mail: wangzd@mater.ustb.edu.cn; Zidong WANG, E-mail: chenxh@skl.ustb.edu.cn*

Abstract:
The Ni-based Udemit720Li superalloy tends to form large γ/γ' eutectic on grain boundaries (GBs) during solidification due to the addition of excessive Al and Ti elements, which provides convenience to study the effect of carbide and γ/γ' eutectic on crack initiation and propagation during tensile process. In this paper, Udemit720Li superalloy samples were prepared by induction melting casting method, arc melting and suction casting method. The microstructure, tensile properties and mechanism of crack initiation and propagation in Ni-based superalloy fabricated by two methods are investigated. The results exhibit γ/γ' eutectic accelerates the stress concentration at GB and thus leads to premature fracture failure. The samples with grain-boundary eutectic have higher strain hardening rate, but their cumulative and local misorientations are lower. For samples without eutectic at GB, the primary crack initiates at grain-boundary carbide along GB and extends along GB or into grain matrix, and exhibits better deformation performance and dislocation storage capacity within grains.

***Keywords:** Superalloy; Carbides; Eutectic; Crack*

1 Introduction

Ni-based superalloy has excellent strength, creep, fatigue and corrosion resistance, which is widely used in high-temperature parts of gas turbine, such as turbine disk and combustion chamber [1,2]. The excellent high-temperature strength mainly arises from the precipitation of ordered and coherent γ' (Ni_3Al) phase in the solid solution matrix [3]. Udimet720Li (developed from Udimet720) alloy is a γ' reinforced alloy developed in the late 1970s [4] that operates at higher temperature (~730℃) than other nickel-base alloy turbine disk. The alloying method is the most widely used method in the microstructure and mechanical properties of Ni-based superalloy. Compared with Udimet720, carbon and boron contents are reduced in Udimet720Li to reduce carbide and boride stringers and improve the forgeability, thus avoiding the need for powder processing [5,6]. Moreover, chromium content decreases from 18 to 16 wt. % to enhance tissue stability and prevent the formation of σ phase, so there is less likely of mechanical properties degradation during high temperature service [7]. The additions of Al and Ti (up to 7.5 wt. %) cause the severe segregation and large precipitation of γ/γ' eutectic in the interdendritic region while significantly increasing the volume fraction of γ' phase [8]. It was acknowledged from alloying experiments that the excellent mechanical properties of Udimet720Li superalloy are mainly come from the precipitation hardening effect of γ' phase (L12 ordered $Ni_3(Al,Ti)$ particles) and M(C,N) (carbon-nitride precipitates) within grain and at GBs [9-11].

In general, the researches demonstrate that the factors affecting the mechanical properties of polycrystalline Ni-based superalloy include precipitates phase, grain size and GB, etc. Microstructures have different effects on the mechanical properties of polycrystalline nickel base superalloy [12,13]. Yan et al. [14] studied the microstructure and lateral properties of a directionally solidified (DS) superalloy with different amounts of boron added. It was found that after solution heat treatment, a γ' cladding was formed around the carbides in boron-containing alloys, which significantly improves transverse creep life and tensile properties at room temperature and 870 ℃. Chang et al. [15] found that γ/γ' eutectic preferentially consumed Al and Ti in the melt and pushed B and Zr into the final solidified melt, resulting in the formation of coarse γ/γ' eutectic structure, η phase and boride in the final solidification stage. Pang et al. [16] studied the influence of

initial microstructure on fatigue crack initiation and short crack propagation at room temperature and found that smaller grain size and coherent γ' phase particle size and higher volume fractions of γ' precipitates improved overall fatigue lifetimes in Udimet720Li superalloy. However, coarsening of grain and secondary γ' precipitates decreases strength and ductility both at room temperature and 400℃ [17]. Previous researches focused on the precipitation of phase during the solidification of Udemit720Li superalloy [8,15], the effect of grain size on properties [16,18], and the tensile properties of heat treated state [17,19]. Although carbide and γ/γ' eutectic have been determined to cause stress concentration which is a dominant factor for cracking, there is still no clear explanation on the role of carbides and γ/γ' eutectic in crack initiation and propagation.

In addition, researchers are committed to optimize the microstructure to simultaneously improve the strength and ductility of materials. Traditional methods to enhance strength are grain-refined strengthening, solution strengthening, dispersion strengthening and strain strengthening. For example, when the grain size is greater than 1 μm, grain refinement can often increase strength without causing a significant decrease in ductility [20-22]. However, traditional strengthening methods can cause dislocations to interact with internal barriers (such as solution atoms, dispersed particles, and GBs) and often reduce plasticity [20]. In particular, owing to the local concentration of internal stress, particles in micron size are the positions priority for crack nucleation, in particular to the particles segregated at GBs, thus considerably reducing ductility and fatigue strength [23-26]. Reasonable ways for optimizing the trade-off between strength and ductility are to take into account the fact that features that not only impede dislocation but also to withstand plastic strain should be strengthened [27,28]. Therefore, it is of great significance to explore and study the mechanism of its strengthening strength and ductility. Regulating the microstructure of material, such as a certain degree of grain refinement, precipitation refinement and the elimination of the brittle segregation is considered to be a reasonable approach for optimizing the strength and ductility trade-off.

The cooling rate is an important influence on the solidification process and microstructure of Ni-base superalloy [29-31], and the evolution of microstructure with cooling rate is closely related to the precipitation behavior of the phases. As a superalloy, Udemit720Li tends to form large γ/γ' eutectic microstructure on GBs during solidification due to the addition of excessive Al and Ti elements, which provides convenience to study the effect of carbide and γ/γ' eutectic microstructure on crack initiation and propagation during tensile process. In this paper, induction melting casting method and arc melting suction casting method were used to fabricate Udemit720Li superalloy samples, respectively. Arc melting and suction casting method have fast cooling. By comparing the tensile properties of the microstructures in alloys fabricated by two method, and the local misorientation after stretching was analyzed by electron backscatter diffraction (EBSD) technique, the effect of carbides and γ/γ' eutectic on crack initiation and propagation was determined.

2 Experimental procedures

The nominal compositions of Udemit720Li superalloy is listed in Table 1. In this study, cylindrical ingot of Φ5070 mm was produced by vacuum induction melting and casting in air-cooled steel mold, labeled as sample A; cuboid ingot of 151560 mm was produced by vacuum arc melting and suction casting in water-cooled copper mold, labeled as sample B. Induction melting and casting were conducted in medium frequency induction furnace with an ultimate vacuum level of 6.0 10^{-2} Pa. Pure Ni, Cr, Co, Mo, W (with a purity of 99.95%, 99.98%, 99.97%, 99.95%, 99.95%, respectively) were first introduced into a corundum crucible located in the vacuum chamber. It is noted that W and Mo were placed at the bottom of the crucible to accelerate diffusion melting. After being evacuated to 5 Pa, the chamber temperature was increased from room value to 1550 ℃, and the temperature was maintained for 20 min. Then, argon was flow into the chamber to increase the chamber pressure to 0.07 MPa, and the bulk Al, Ti and the aluminum foil wrap B, Zr was then added to the melt. After homogenizing, the furnace temperature was reduced to 1450 ℃ and hold for 10 min. Finally, the melt was poured into the steel mold and natural cooling. The cooling rate of the alloy in steel mold was less than 100 K/s. In addition, arc melting and suction casting were processed by arc-melting furnace with an ultimate vacuum level of 5.0 10^{-3} Pa. 50 g bulk was cut from sample A for arc melting. Electromagnetic stirring was conducted during the melting process to ensur e the uniformity of components. After melted, the alloy was drop-cast into the water-cooled cupper mold and cooling rate more than 1000 K/s.

Table 1 Material compositions in wt%.

Composition	C	Cr	Co	W	Mo	Al	Ti	B	Zr	Ni
Content	0.015	16	14.75	1.25	3	2.5	5	0.015	0.03	Bal.

The metallographic and “dog-bone plate tensile were EDM (Electric Discharge Machining) wire cutting process from 1/2 radius of cylindrical ingot and 1/4 cuboid ingot as show in figure 1.

The tensile tests were carried out on a CMT4105 testing machine according to the GB/T 228.1-2010. The tensile speed and temperature was set as 1mm/min and 21 ℃, respectively. After tensile testing, longitudinal section was cut from the fractured specimens. The specimens were ground, polished and chemical etched and then characterized by using SEM to observe the propagation path of crack and the evolution of crack in the longitudinal section.The as-cast microstructure, tensile fracture and longitudinal section of two samples were studied by optical microscopy (OM), scanning electron microscopy (SEM) and electron backscatter diffraction (EBSD). The metallographic specimens were ground through 400 to 2000 grit papers, polished with diamond paste, cleaned by ultrasonic device. And then the specimens were chemically

etched using a solution of 5g $CuCl_2$ + 100 ml C_2H_5OH + 100ml HCl for OM examination or electro etched with 13 ml H_3PO_4 + 42 ml HNO_3 + 43 ml H_2SO_4 at 6V for 5~10s at room temperature for SEM examination. For EBSD samples, the specimens were electro-polished with 10 ml H_4ClO_4 + 90 ml C_2H_5OH at 29V for 5s at room temperature, and the EBSD investigation was performed on the sample by using a LEO1450 scanning electron microscope equipped with HKL Channel 5, to observe the grain size, grain orientation and the plastic deformation distribution after tensile tests.

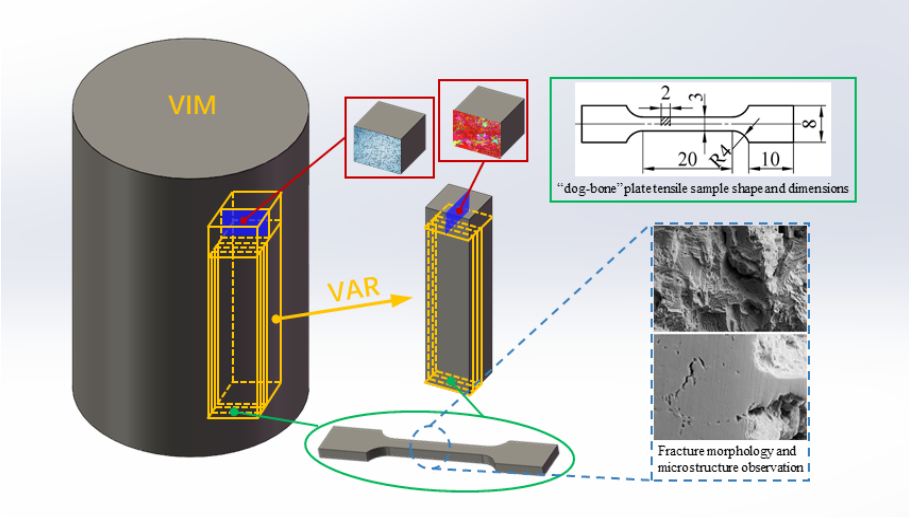

Figure 1 Schematic illustration of Udimet720Li metallographic and "dog-bone" plate tensile

3 Results and discussion

3.1 Microstructure of the as-cast Udimet720Li superalloy

Figure 2 displays the low magnification OM image of microstructure by two casting method. It is obvious that sample A shows larger grain size of equiaxed crystals accompanied by local dendrites, and fan-type γ/γ' eutectic, block-shaped and strip-shaped η-Ni_3Ti are distributed at GBs (figure 2a, c), consistent with the as-cast microstructure of Uidmet720Li [8]. The macrostructure images of sample B show extremely fine grain size and fine MC carbides discontinuously distributing at GB, with no common γ/γ' eutectic structure (figure 2b, d).

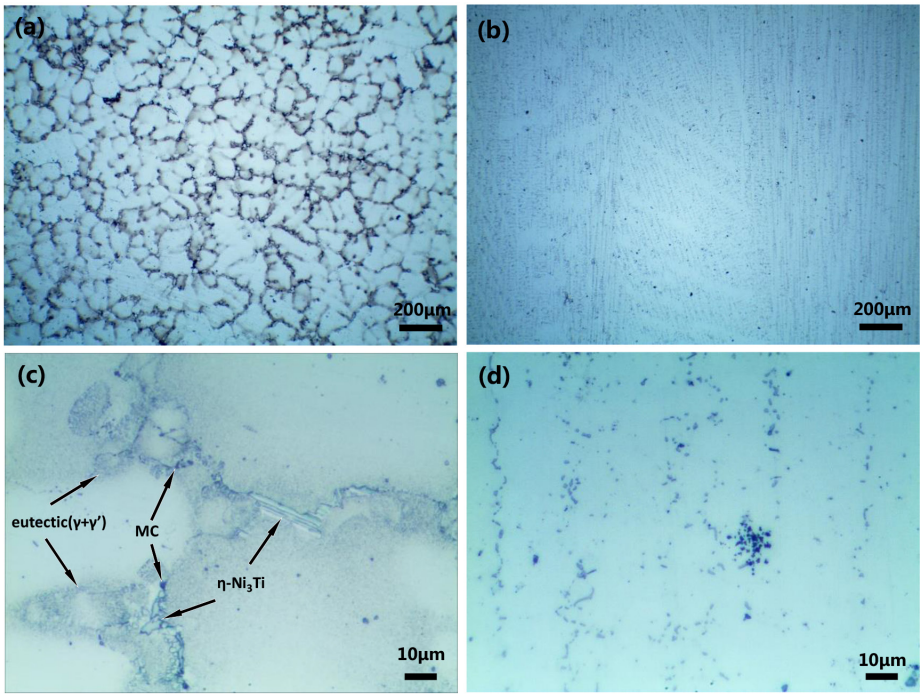

Figure 2 Low magnification OM image of alloying microstructure in (a) sample A and (b) sample B; (c) fan-type γ/γ' eutectic, block-shaped and strip-shaped η-Ni3Ti distributed at GB of sample A; (d) fine MC carbides discontinuously distributed at the GB of sample B.

In SEM images, the γ' particles are observed dispersed in the grain matrix of in samples A and B. As shown in figure 3b, the size of γ' precipitate increases from the grain center to the GB, and γ' particles in sample A are finer than those in sample B. In addition to the fan-type γ/γ' eutectic, block-shaped and strip-shaped η-Ni_3Ti, there are also a series of granular MC carbides at the GB of sample A (figure 3a). However, γ/γ' eutectic rarely appears at the GB of sample B, and it can be observed irregular phases are intermittently distributed at the GB (figure 3c). Trough EDS analysis (figure 4), it can be ascertained that the irregular phases is TiC (figure 3d). It is reported that the formation of γ/γ' eutectic mainly depends on the segregation of titanium [32]. The few eutectic in as-cast microstructure of sample B, different from sample A, can be attributed to the rapid solidification of arc melting and suction casting method, which prevents the segregation of titanium at the GB to form γ/γ' eutectic. Furthermore, γ/γ' eutectic tends to aggregate at the triple GB junctions, in which more titanium is enriched. In contrast, the enrichment of titanium at general GBs is not enough to produce the γ/γ' eutectic.

The orientation image microscopy map of the two samples in figure 5 shows quite difference in grain size.

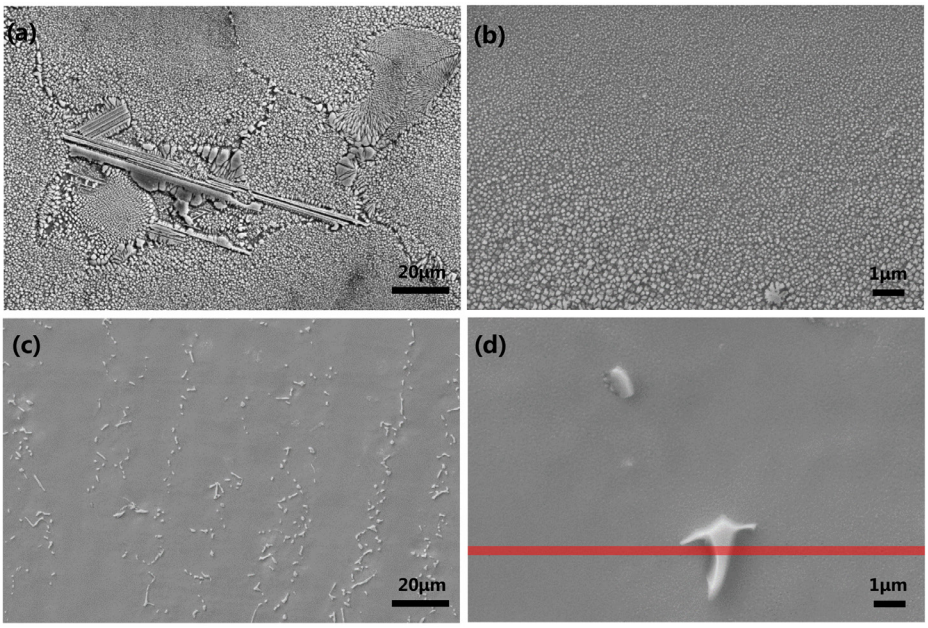

Figure 3 SEM image of two as-cast microstructures: (a) the phases and structure of GB in sample A; (b) the size of γ' distribution in grain of sample A; (c) irregular phase intermittently distributed at GB in sample B, (d) irregular phase in sample B determined by EDS as TiC.

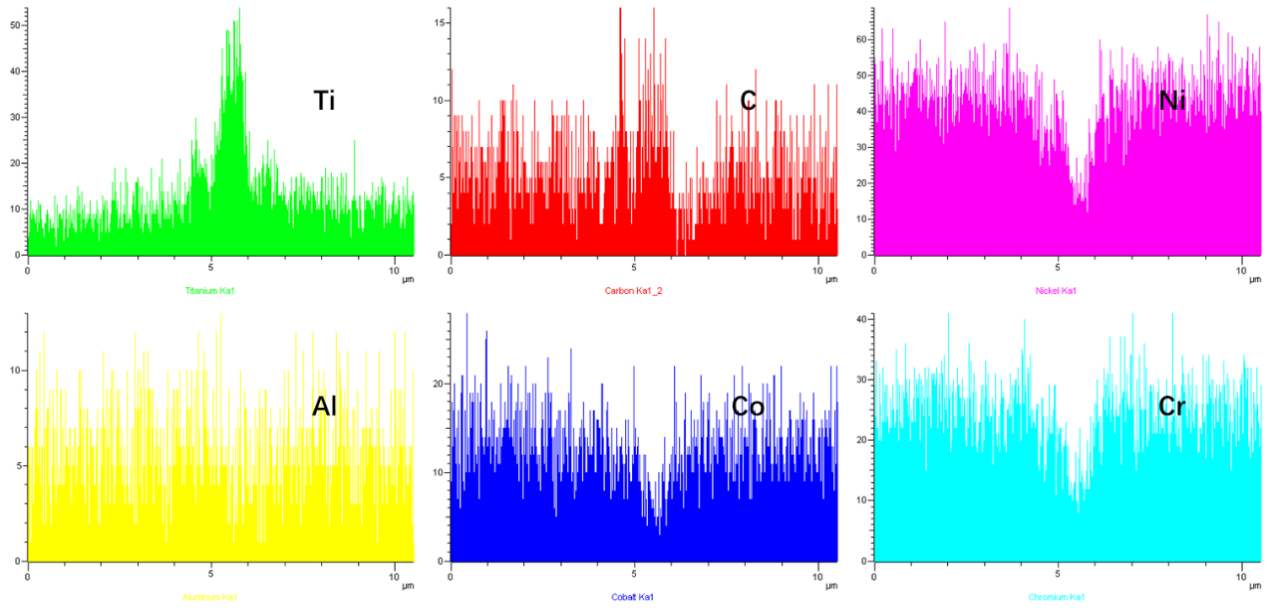

Figure 4 Element distribution along the red line marked in Fig 3d

By the line interception method, the average grain sizes in samples A and B are determined as 74.6 and 36.4 μm, respectively. Here, different color levels in the orientation image micrograph represent different crystal orientations, thin-gray lines and thick-black lines represent LAGBs and HAGBs, respectively.

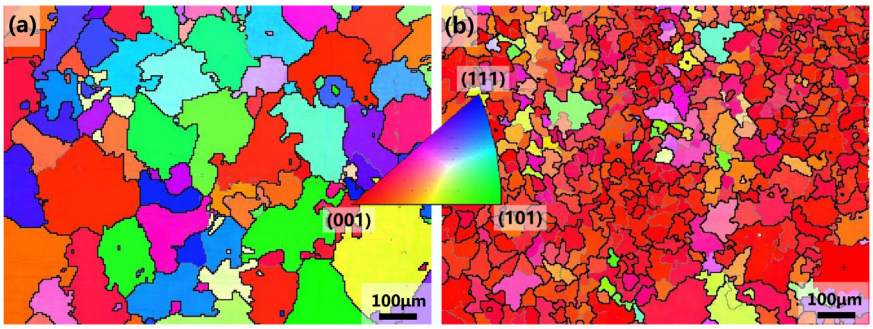

Figure 5 Orientation image microscopy map of (a) sample A and (b) sample B

3.2 Tensile behavior of the as-cast Udimet720Li superalloy

Tensile tests were performed on Udimet720Li superalloy at room temperature, and the results are shown in Table 2. It can be found, compared with sample A, the yield strength (σ_s), ultimate tensile strength (σ_{UTS}) and elongation (δ_u) of sample B are enhanced. Sample A displays the lower strength and ductility, which is most likely caused by its coarse and uneven microstructure in terms of grains and phases at GB (figure 3a and figure 5a). For sample B, attributed to suction casting in water-cooled copper mold, finer grains and particle phases at GB lead to substantial elevations in the σ_s from of 826-939 MPa, and in the δ_u from of 12-15%. In addition, the strain hardening rate of sample A is higher than that of sample B during tensile deformation (figure 6). Dislocations accumulate when they intersected or by-passed the γ' particles, which induces enhanced strain hardening. However, the uniform elongation of sample A is lower than sample B. Although sample A has a higher strain hardening rate than sample B, but premature fracture occurs.

Table 2 Mechanical performance of samples A and B

Samples	σ_s(MPa)	σ_{UTS}(MPa)	δ_u(%)
A	826	1156	12
B	939	1213	15

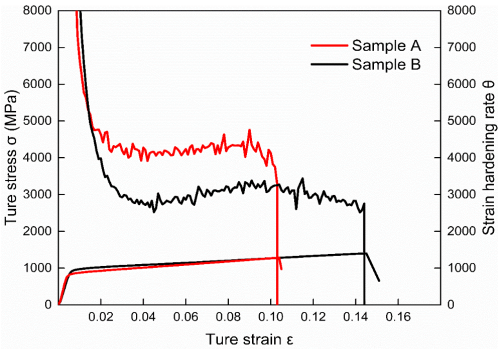

Figure 6 Comparison of room-temperature tensile behavior for the samples

red and black lines are tensile true stress-strain curves and hardening rate-strain curves of samples A and B, respectively. Strain hardening rate $\theta = d\sigma / d\varepsilon$

3.3 Crack and deformed microstructure of Udimet720Li superalloy after tensile test

Samples A and B both demonstrate a combination of ductile and brittle fracture mechanisms, respectively with dimples and quasi-cleavage facets. The number of dimples in the fracture surface of sample A is significantly less than sample B. In SEM images of fracture surface (figure 7) and cross-section microstructure of fracture tips (figure 8), the crack is mainly generated at the GB at which brittle carbon act as a crack source. The crack growth and fracture mode are different between the two samples. For sample B (figure 7b, d and f), micro-fracture shows many dimple and tearing ridge basically dendrite fracture, and the proportion of dimple is dominant. The primary crack originates from carbide at GB due to intermittent existence of carbide, and secondary crack extends along the GB or into grain matrix, so that crack propagation is hindered by intragranular γ' precipitation [33]. The strip tearing ridge of fracture surface is a sign of rapid crack growth. At the same time, the existence of massive phases can be observed at the end of each tearing ridge, which is the carbide at the GB through EDS analysis. It can be concluded, the brittle carbides distributed at the GB can act as the crack source, but can also hinder the dislocation slip between grains. For sample A (figure 7a, c and e), macro fracture is composed of fiber zone and shear lip zone. Fiber zone area has a lot of intergranular or transgranular fracture planes and some tearing dimples, and the proportion of dimple is inferior. Primary crack originate from carbide at GB tends to extend to γ/γ' eutectic (figure 8). Fan type γ/γ' eutectic has a petal or lamellar shape and always leads to phenomenon of delamination and peeling of eutectic because of poor deformation coordination between eutectic layers, as shown in figure 8a. This delamination will reduce the dislocation pinning ability of strengthening phase at GB and causing premature fracture, thus reduce the ultimate strength.

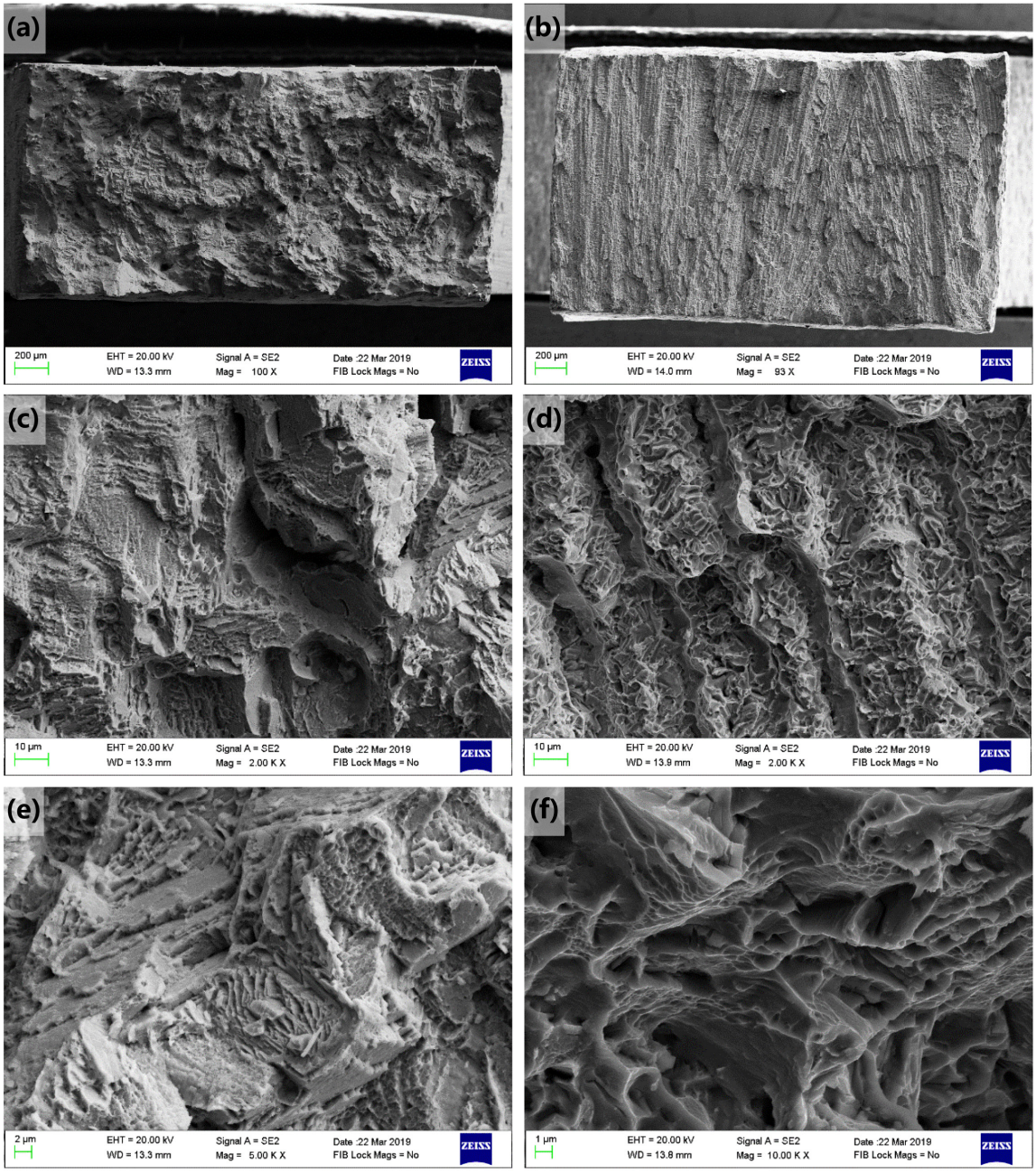

Figure 7 Fractographs of specimens under room-temperature tensile test: (a), (c) and (e) sample A; (b), (d) and (f) sample B

3.4 Electron backscatter diffraction of cross section of fracture tips

In order to study the tensile deformation mechanism, electron backscatter diffraction (EBSD) was used to analyze the plastic deformation of the cross section of fracture tips. EBSD can be used to study the relationship between microstructure and plastic deformation, and analyze the distribution of plastic deformation in polycrystalline alloy [34,35]. The applied stress causes dislocation migration and plastic deformation in the alloy, and inhomogeneous distribution of dislocation in grains will lead to inhomogeneous plastic deformation, resulting different local misorientation within grains [36]. Local misorientation images can reflect the distribution of plastic deformation. The distribution of plastic deformation in polycrystalline alloy can be clearly revealed by comparing All Euler image and Local misorientation image.

The microstructure near the tensile fracture surface analyzed by EBSD plane scanning are shown in figure 9. The local misorientation of sample A tends to gather at the GB and the crystal is relatively small, which indicates that the plastic deformation mainly occurs at GB and the plastic deformation in crystal is relatively small (figure 9a, c). Meanwhile, triple GB junctions often has more large misorientation, at which the plastic deformation is greater

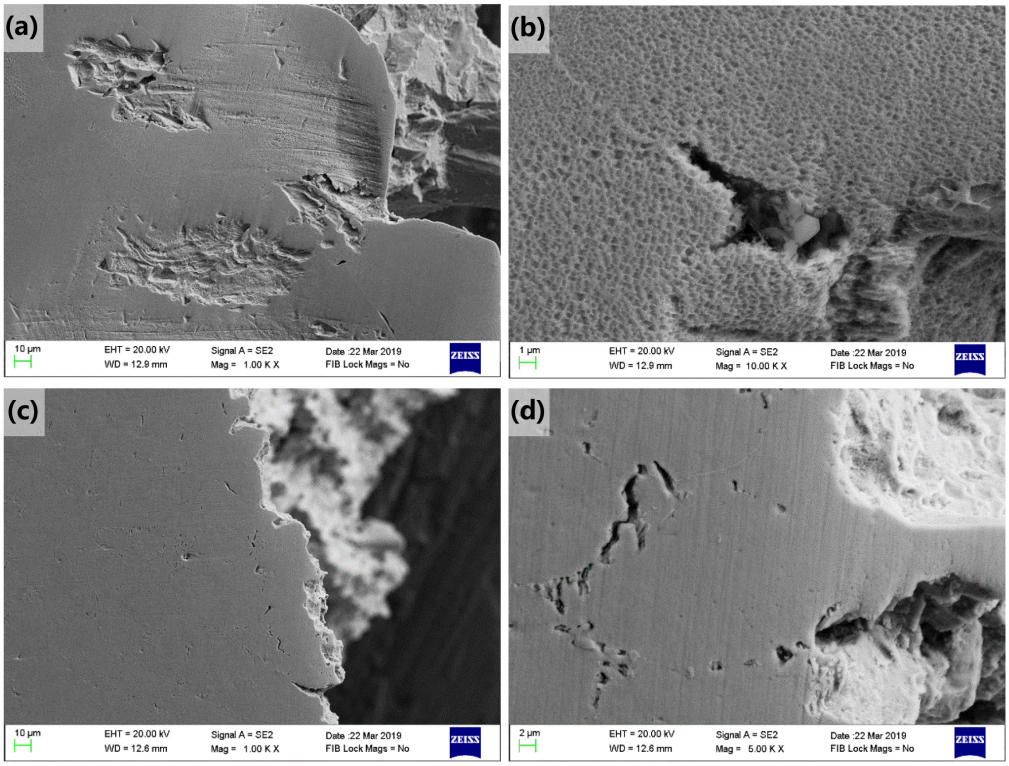

Figure 8 Micrographs of cross section of fracture tips for room-temperature tensile test (a) and (b) sample A; (c) and (d) sample B.

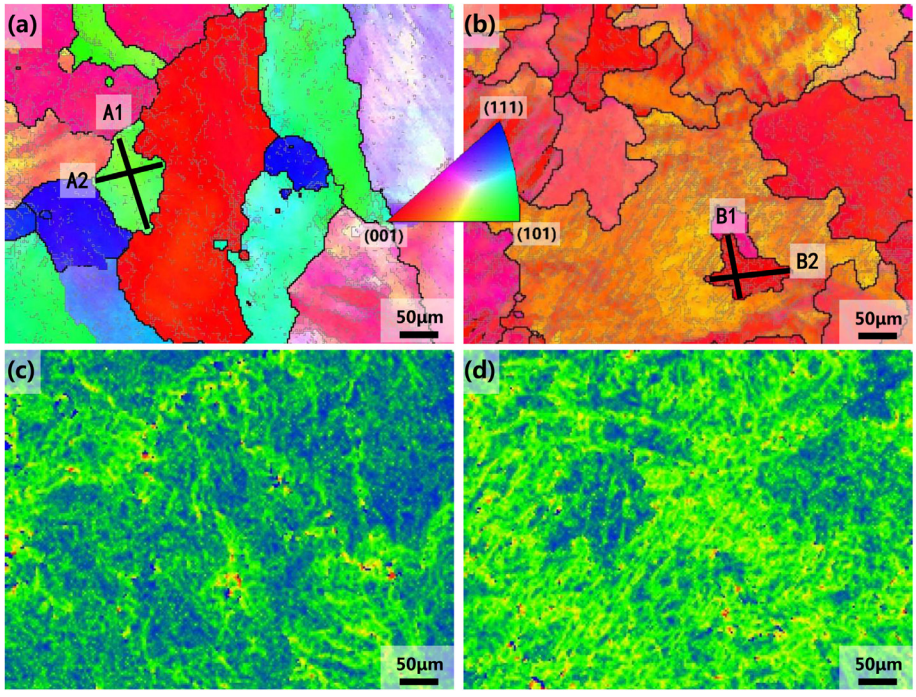

Figure 9 EBSD plane sweep scanning images near the tensile fracture: (a), (b) IPF image; (c), (d) Local Misorientation image. (The misorientation increases from blue to rad).

and stress concentration is also more serious. In as-cast structure, the γ/γ' eutectic usually solidifies at the triple GB junctions. For sample B, there is a different situation. As shown in figure 9b, d, the misorientation is almost uniformly distributed in a single grain and no significantly different between crystal and GB. These results confirm previous conclusion that γ/γ' eutectic at GB causes premature stress concentration and leads to premature fracture failure of the material.

To evaluate quantitatively the transformation of

orientation difference between two samples, the point to origin (cumulative) misorientation and point to point (local) misorientation are calculated along the lines marked in figure 9a, b. The misorientation profiles along the directions of lines A1 and A2 are illustrated in figure 10a, b. The cumulative misorientation is around 6 and average local misorientation is 1 of sample A. As shown in figure10 c, d, an increased misorientation gradient near the GB is developed, and the cumulative misorientation along line B1 and B2 exceeds 8° for a distance about 100μm. Therefore, it can be concluded that the misorientation in the grain of sample A is less than that of sample B. In other words, sample B has better deformation performance and dislocation storage capacity in grains. However, as shown in figure 10, the distance from grain interior to GB, the local misorientation does not increase monotonically. The obvious misorientation jumps appear at all range. According previous study, this is related to the activation of different slip systems [37]. Original grain has several orientation bands, and compatible deformation between adjacent grains takes place by activating different slip systems.

Although sample B has a low strain hardening rate at large strains during deformations, but shows stronger work hardening stability. High strain rates led to a large number of dislocations during tensile tests at room temperature, while high hardness phase and carbide resulted in dislocation accumulation in the crystal channels and phase interfaces. In general, numerous dislocations segregated at the interface of matrix/carbide and matrix/eutectic cause stress concentration along these phase interface. For sample A, the cross section of fracture tips shows delamination and peeling of γ/γ' eutectic (figure 8a, b). Different from sample A, sample B cross section of fracture tips shows source of crack is carbide (figure 8c, d). As shown in the EBSD results in figure 9c, d, compared with sample B, the narrow and small strain concentration region near GB indicates that the stress required for GB cracking of sample A is small. As a result, the stress concentration caused by the GB would be large, and the microcrystalline crack of samples A and B tends to nucleate at carbide and γ/γ' eutectic at the GBs.

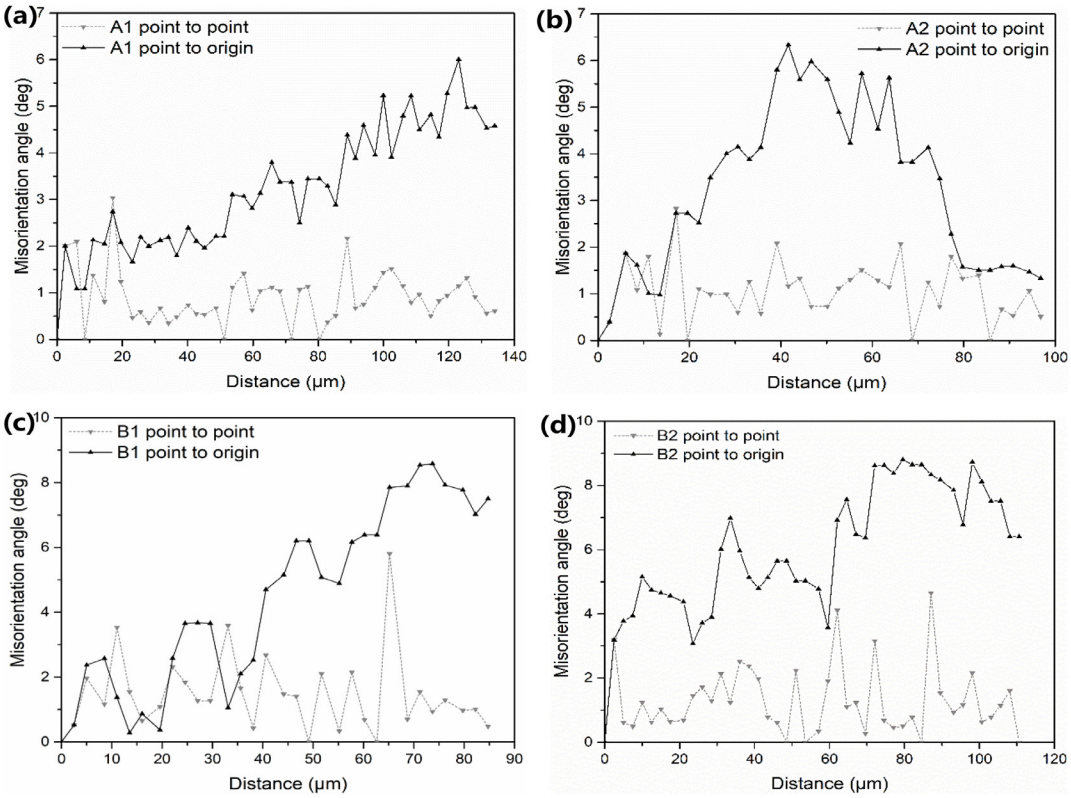

Figure 10 Change of misorientation angle along the lines marked in Figure 9 (a) A1; (b) A2; (c) B1; (d) B2

4 Conclusions

The microstructure and mechanisms of tensile cracks initiation and propagation in Ni-based superalloy fabricated by two methods are investigated. The results can be concluded as follows:

(1) Sample B has a finer grain size and less eutectic content due to its rapid solidification. Various phases are distributed at GBs for sample A, but only the single Ti-rich carbide dispersed at GBs of sample B.

(2) The strain hardening rate of sample A is higher than sample B, but the uniform elongation is lower in the former due to the premature fracture during deformation.

(3) The cumulative and local misorientations in sample A are less than those in sample B, which indicates that sample B has better deformation performance and dislocation storage capacity in grains. In terms of crack initiation and propagation, γ/γ' eutectic accelerates the

stress concentration at GB and leads to premature fracture failure.

Acknowledgments: This work was supported by the USTB University of Science and Technology Beijing.

References

[1] Kim S E, Jackson M P, Reed R C, et al. Quantification of the minor precipitates in UDIMET™ alloy720(LI) using electrolytic extraction and X-ray diffraction 1[J]. Materials Science & Engineering A, 1998, 245(2):225-232.

[2] Yongchang L, Qianying G, Chong L I, et al. Recent progress on evolution of precipitates in Inconel 718 superalloy [J]. Acta Metallurgica Sinica, 2016.

[3] Mao J, Chang K M, Yang W, et al. Cooling precipitation and strengthening study in powder metallurgy superalloy U720LI[J]. Metallurgical & Materials Transactions A, 2001, 32(10):2441-2452.

[4] F E Sczerzenie, G E Maurer. Development of Udimet 720 for High Strength Disk Applications[J]. Special Metals Corporation, 1984

[5] P W Keefe, S O Mancuso, G E Maurer. Effect of heat treatment and chemistry on the long-term phase stability of a high strength nickel-based superalloy[J]. Superalloys, 1992, 487-496

[6] Bain K R, Gambone M L, Hyzak J M, et al. Development of Damage Tolerant Microstructures in Udimet 720[C]// Superalloys. 1988.

[7] Na Y S, Park N K, Reed R C. Sigma morphology and precipitation mechanism in udimet 720Li[J]. Scripta Materialia, 2000, 43(7):585-590.

[8] Zhao G D, Yu L X, Qi F, et al. The Minor Precipitation at the Final Stage of U720Li Solidification[J]. Acta Metallurgica Sinica, 2016, 29(6):518-526.

[9] Li F, Fu R, Yin F, et al. Impact of γ'(Ni3(Al,Ti)) phase on dynamic recrystallization of a Ni-based disk superalloy during isothermal compression[J]. Journal of Alloys & Compounds, 2017, 693:1076-1082.

[10] Joseph C, Persson C, Colliander M H. Influence of heat treatment on the microstructure and tensile properties of Ni-base superalloy Haynes 282[J]. Materials Science and Engineering: A, 2016:S0921509316312618.

[11] Liu F, Chen J, Dong J, et al. The hot deformation behaviors of coarse, fine and mixed grain for Udimet 720Li superalloy[J]. Materials Science and Engineering: A, 2016, 651:102-115.

[12] Du B, Sheng L, Cui C, et al. Precipitation and evolution of grain boundary boride in a nickel-based superalloy during thermal exposure[J]. Materials Characterization, 2017, 128:109-114.

[13] Osada T, Gu Y, Nagashima N, et al. Optimum microstructure combination for maximizing tensile strength in a polycrystalline superalloy with a two-phase structure[J]. Acta Materialia, 2013, 61(5):1820-1829.

[14] Yan B C, Zhang J, Lou L H. Effect of boron additions on the microstructure and transverse properties of a directionally solidified superalloy[J]. Materials Science & Engineering A, 2008, 474(1-2):39-47.

[15] Chang L, Jin H, Sun W. Solidification Behavior of Ni-base Superalloy Udimet 720Li[J]. Journal of Alloys & Compounds, 2015.

[16] Pang H T, Reed P A S. Effects of microstructure on room temperature fatigue crack initiation and short crack propagation in Udimet 720Li Ni-base superalloy[J]. International Journal of Fatigue, 2008, 30(10-11):2009-2020.

[17] Zhipeng W, Lianxi H, Yu S, et al. Effect of solution treatment on microstructure and tensile properties of a U720LI Ni-based superalloy[J]. Vacuum, 2018, 156: 248-255

[18] Villechaise P, Cormier J, Billot T, et al. Mechanical Behavior and Damage Processes of Udimet 720Li: Influence of Localized Plasticity at Grain Boundaries[M]// Superalloys 2012.

[19] Rao G A, Satyanarayana D V V. Influence of HIP processing on microstructure and mechanical properties of superalloy Udimet 720LI[J]. Materials Science & Technology.

[20] Lu K. The Future of Metals[J]. Science, 2010, 328:319-320.

[21] M. A. Meyers, A. Mishra, D.J. Benson, Mechanical properties of nanocrystalline materials, Progress in Materials Science. 51: 427-556.

[22] Lu K. Stabilizing nanostructures in metals using grain and twin boundary architectures[J]. Nature Reviews Materials, 2016, 1(5):16019.

[23] Valiev R Z. Nanostructured alloys: Large tensile elongation[J]. Nature Materials, 2013, 12(4):289-291.

[24] Liu G, Zhang G J, Jiang F, et al. Nanostructured high-strength molybdenum alloys with unprecedented tensile ductility[J]. Nature Materials, 2013, 12(4):344-350.

[25] Launey M E, Ritchie R O. On the Fracture Toughness of Advanced Materials[J]. Advanced Materials, 2009, 21(21):2103-2110.

[26] Kaixuan C, Xiaohua C, Zidong W, et al. Optimization of deformation properties in as-cast copper by microstructural engineering. Part I. microstructure[J]. Journal of Alloys and Compounds, 2018, 763:592-605.

[27] Lu K, Lu L, Suresh S. Strengthening Materials by Engineering Coherent Internal Boundaries at the Nanoscale[J]. SCIENCE, 2009, 324(5925):349-352.

[28] Chen K X, Chen X H, Ding D, et al. Effect of in-situ nanoparticle wall on inhibiting segregation of tin bronze alloy[J]. Materials Letters, 2016, 175:148-151.

[29] Seo S M, Lee J H, Yoo Y S, et al. A Comparative Study of theγ/γ'Eutectic Evolution During the Solidification of Ni-Base Superalloys[J]. Metallurgical & Materials Transactions A, 2011, 42(10):3150-3159.

[30] Bingming G, Lin L, Xinbao Z, et al. Effect of Directional Solidification Methods on the Cast Microstructure and Grain Orientation of Blade Shaped DZ125 Superalloy[J]. Rare Metal Materials and Engineering, 2013, 42(11):2222-2227.

[31] Liu L, Huang T W, Zhang J, et al. Microstructure and stress rupture properties of single crystal superalloy CMSX-2 under high thermal gradient directional solidification[J]. Materials Letters, 2007, 61(1):227-230.

[32] Seo S M, Lee J H, Yoo Y S, et al. A Comparative Study of the γ/γ' Eutectic Evolution During the Solidification of Ni-Base Superalloys[J]. Metallurgical & Materials Transactions A, 2011, 42(10):3150-3159.

[33] Wang Q, Ding H, Zhang H, et al. Variations of microstructure and tensile property of γ-TiAl alloys with 0~0.5 at% C additives[J]. Materials Science and Engineering A, 2017, 700:198-208.

[34] Kuhn F, Zeismann F, Brueckner-Foit A. Crack growth mechanisms in an aged superalloy at high temperature[J]. International Journal of Fatigue, 2014, 65:86-92.

[35] Miao J, Pollock T M, Jones J W. Microstructural Extremes and the Transition from Fatigue Crack Initiation to Small Crack Growth in a Polycrystalline Nickel-base Superalloy[J]. Acta Materialia, 2012, 60(s 6–7):2840–2854.

[36] Jiashi Miao, Tresa M Pollock, J Wayne Jones. Crystallographic fatigue crack initiation in nickel-based superalloy René 88DT at elevated temperature[J]. Acta materialia, 2009, 5946-5974

[37] Randle V , Hansen N , Jensen D J . The deformation behaviour of grain boundary regions in polycrystalline aluminium[J]. Philosophical Magazine A, 1996, 73(2):265-282.